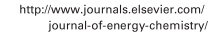


Contents lists available at ScienceDirect

## Journal of Energy Chemistry



journal homepage: www.elsevier.com/locate/jechem

# Sulfur-resistant methanation over MoO<sub>3</sub>/CeO<sub>2</sub>–ZrO<sub>2</sub> catalyst: Influence of Ce-addition methods

Zhaopeng Liu, Yan Xu, Zhenhua Li, Baowei Wang\*, Weihan Wang, Xinbin Ma\*, Renjie Liu

Key Laboratory for Green Chemical Technology of Ministry of Education, School of Chemical Engineering and Technology, Collaborative Innovation Center of Chemical Science and Engineering (Tianjin), Tianjin University, Tianjin 300072, China

## ARTICLE INFO

Article history:
Received 17 June 2017
Revised 5 October 2017
Accepted 7 October 2017
Available online 14 October 2017

Keywords: Sulfur-resistant methanation Ce introducing methods Reducible Ce<sup>3+</sup> Synthetic natural gas Active MoS<sub>2</sub>

#### ABSTRACT

In this paper,  $Ce_{0.2}Zr_{0.8}O_2$  composite supports were prepared by different Ce-addition methods including impregnation of cerium (CeZr-imp), impregnation of citric acid and cerium (CeZr-CA) simultaneously and deposition precipitation method (CeZr-DP), respectively. The as-prepared supports were applied to prepare 10 wt%  $MoO_3/Ce_{0.2}Zr_{0.8}O_2$  catalysts for sulfur-resistant methanation. The  $N_2$  adsorption/desorption, X-ray diffraction (XRD), Raman spectroscopy (RS), X-ray photoelectron (XPS), temperature-programmed reduction by hydrogen ( $H_2$ -TPR) were undertaken to get textural properties, morphological information and structures of the catalysts. The results showed that  $MoO_3$  was highly dispersed on the surface of these three supports and Ce was mostly of coexisted in  $Ce^{4+}/Ce^{3+}$  redox pairs. Compared with Mo/CeZr-imp, the CO conversion increased by 10% and 15% for Mo/CeZr-CA and Mo/CeZr-DP, respectively. This was mainly attributed to the larger specific surface area,  $Ce^{3+}$  concentration and content of active  $MoS_2$  on the surface of catalysts.

© 2017 Science Press and Dalian Institute of Chemical Physics, Chinese Academy of Sciences. Published by Elsevier B.V. and Science Press. All rights reserved.

#### 1. Introduction

With attention to environmental protection, natural gas viewed as a clean and efficient energy is not only optimizing the energy structure, easing the energy supply and demand, but also improving the quality of the environment and sustainable development. Whereas, the serious shortage of natural gas restricts the development of economy and society, as well as the concern on the depletion of natural gas [1-4]. Synthetic natural gas (SNG) produced from coal or biomass is considered again. Furthermore, due to energy crisis and the severer environment pollution problems all over the world, SNG production primarily originated from coal was deemed to a type of clean energy source that facilitates a more rational use of coal resources. Methanation is a main process used to produce SNG from coal. In general, supported Ni catalyst, with the high conversions of CO and good selectivity to CH<sub>4</sub> has been widely employed during the methanation reaction [5]. The methanation reaction over Ni-based catalysts occurs as follows:

$$CO + 3H_2 \rightarrow CH_4 + H_2O$$
  $\Delta H = -2.10 \times 10^5 \text{ kJ/kmol}$  (1)

The stoichiometric relationship of Eq. (1) indicates that methanation process over Ni-based catalysts always occur when the mo-

lar ratio of  $H_2/CO$  was higher than 3, but this ratio is difficult to generate for most gasification processes. It is reported that the  $H_2/CO$  ratio can be adjusted by water-gas shift (WGS) reaction (see Eq. (2)). What was worse, Ni-based catalysts are very sensitive to sulfur content as it can cause serious poisoning of the active phases [6,7]. Therefore, this required through the stringent desulfurization process to control sulfur content no more than 0.1 ppm before methanation process.

$$CO + H_2O = CO_2 + H_2O \quad \Delta H = -4.10 \times 10^4 \text{ kJ/kmol}$$
 (2)

Compared to the Ni catalyst, Mo-based catalysts with methanation activity, WGS activity and sulfur resistance has drawn the increasing attention processes. That is to say that Mo-based catalysts are active in the condition of low  $\rm H_2/CO$  ratio as 1:1 [8,9]. For sulfur-resistant methanation based on  $\rm MoO_3$  catalysts there are two viewpoints: Hou and Wise [10] found that sulfur-resistant methanation consist of two basic reactions: synergistically composed by Eq. (1) methanation and Eq. (2) WGS; By contrast, Happel et al. [11] considered that methanation reaction using  $\rm MoO_3$  catalysts maybe coupled with methanation and WGS reaction process which is described as follows:

$$2CO + 2H_2O = CH_4 + CO_2 \quad \Delta H = -1.20 \times 10^5 \text{ kJ/kmol}$$
 (3)

The support plays an important role in sulfur-resistant methanation. A series of supports have been investigated for sulfur-

<sup>\*</sup> Corresponding authors.

E-mail addresses: wangbw@tju.edu.cn (B. Wang), xbma@tju.edu.cn (X. Ma).

resistant methanation of MoO<sub>3</sub> catalysts, for instance, Al<sub>2</sub>O<sub>3</sub> [12,13],  $ZrO_2$  [3],  $CeO_2$  [9,14], and the composite  $CeO_2$ - $Al_2O_3$ [15–18]. Zirconia is an excellent support and has received considerable attention due to its unique properties of high surface area and structural stability [19]. Furthermore, ZrO<sub>2</sub> supported Mobased catalysts were better than alumina-supported counterparts in hydrotreatment reaction [19] resulted from the surface properties and the interactions with molybdenum. As an effective support of catalyst, CeO<sub>2</sub> was widely used for some chemical reactions for its high oxygen storage capacity and its good redox properties associated with the easy translation between Ce<sup>4+</sup> and Ce<sup>3+</sup> oxidation states, such as dry reforming of methane [20] and WGS [21–25] reaction. In addition, CeO<sub>2</sub>-containing supports were widely employed in automotive application in recent years due to its high thermal stability [26]. For zirconium supported Mo-based catalyst, the reducible Ce<sup>3+</sup> may promote formation of defect oxygen and active species. So, it was deduced that CeO2 is a promising support applied in sulfur-resistant methanation [14]. However in our previous work, little information was found about the effect of nature and characteristics of CeO<sub>2</sub>-ZrO<sub>2</sub> composite supports on the sulfur-resistant methanation activity over MoO3 catalysts though some comparative studies of supported MoO<sub>3</sub> catalysts with different carriers have been reported.

In this paper, the different CeO<sub>2</sub>–ZrO<sub>2</sub> composites with different introduction of Ce species were prepared as the supports. Meanwhile the sulfur-resistant methanation activity over supported MoO<sub>3</sub> catalysts was conducted. To better understand the beneficial effects of Ce species on the properties of the catalysts, a series of characterizations were performed. The characterizations results were discussed correlated with the catalytic performance.

## 2. Experimental

## 2.1. Composite support preparation

The  $\rm ZrO_2$  powder was prepared by precipitation method using zirconium nitrate (99.6 wt%, Kermel) and ammonia (25 wt%, Real & Lead) as the agent. Specially, 122 mL zirconium nitrate solution (1 mol/L) was added to 41 mL diluted ammonia (diluted 10 times with deionized water) at 80 °C by stirring for 0.5 h and the mixture was digested at 80 °C for 3 h without stirring, then the solid was isolated by vacuum filtration, washed with deionized water, dried at 120 °C for 12 h and calcined at 600 °C for 12 h.

The composite support of CeZr-imp (with 20 wt% CeO $_2$  in ZrO $_2$ ) was prepared by impregnating cerous nitrate (99 wt%, Kermel) on ZrO $_2$  powder. Certain amounts of cerous nitrate solution was added to 10 g ZrO $_2$  powder (< 180 mesh) with stirring using a glass rod for 3 h. The impregnated sample was kept at room temperature (about 25 °C) for 24 h, subsequently dried at 50 °C for 12 h and 120 °C for 12 h, finally calcined at 600 °C for 4 h with ramp 5 °C /min.

The composite support of CeZr-CA (with 20 wt%  $CeO_2$ ) was prepared by simultaneously impregnating 8 mL citric acid (99.5 wt%, Aladdin) and cerous nitrate solution on 10 g  $ZrO_2$  powder with same procedure as CeZr-imp.

The composite support of CeZr-DP (with 20 wt% CeO<sub>2</sub>) was prepared by a deposition precipitation method. Firstly, the  $\rm ZrO_2$  powder (10 g) was mixed with a certain amount of cerous nitrate solution in a round-bottomed flask. Secondly, an aqueous ammonia solution was added to the above solution drop-wise at 80 °C and then the mixture was digested at 80 °C for 3 h, filtered and washed with deionized water. Finally, the sample was undergone the same thermal treatment as above.

#### 2.2. Catalysts preparation

All catalysts were prepared by impregnating the desired support which was grinded into 180 mesh with aqueous solutions of heptamolybdate (Kermel). The mixtures were continuously stirred at 50 °C and dried at 120 °C for 12 h in air. Then the samples were calcined at 600 °C for 4 h with a heat rate of 5 °C/min. After calcinations, the catalysts were underwent pressurization molding for 1 h by 40 MPa with the pressurization pressing machine (FW-40T). Finally, the catalyst after molding was sized to 20–40 mesh. For all samples, the amount of  $MoO_3$  was about 10 wt% of supports. The catalysts were denoted as: 10Mo/CeZr-imp, 10Mo/CeZr-CA and 10Mo/CeZr-DP, respectively.

## 2.3. Catalysts characterization

#### 2.3.1. N<sub>2</sub>-physisorption

 $N_2$ -physisorption of the supports and catalysts were measured at  $-196~^{\circ}\text{C}$  respectively with a Tristar 3000 apparatus (Micromeritics, United States) with a pretreatment of the  $N_2$ -physisorption analysis, each fresh sample should be degassed at 300  $^{\circ}\text{C}$  for 3 h in vacuum. The BET surface area of samples was calculated by Brunauer–Emmett–Teller (BET) method, and average pore size was obtained by the Horvath–Kawazoe (HK) equation.

## 2.3.2. X-ray diffraction analysis

X-ray diffraction (XRD) was detected on a D/max-2500 X-ray diffraction meter (Rigaku, Japan) with Ni-filtered Cu- $K\alpha$  radiation ( $\lambda=1.541\,$  nm, 40 kV, 20 mA). The diffraction patterns were recorded in the range  $5^{\circ} < 2\theta < 90^{\circ}$  with a scanning rate of  $5^{\circ}$ /min. The XRD phases were identified by comparison with powder diffraction data from the Joint Committee on Powder Diffraction Standards (JCPDS) and the grain size of crystallize was obtained according to the Deby–Scherrer equation.

## 2.3.3. Raman analysis

The Raman spectra Mo/CeZr catalysts were obtained with an InVia-Reflex (Renishaw, Wotton-under-Edge, Gloucestershire, UK) laser Raman spectrometer with high-sensitivity systems of integrated research grade microscopes. The excitation wave-number at 532 nm with an Ar<sup>+</sup>-ion laser (spectra physics) was employed as the incident light beam. The morphologies for the samples were examined by electronic microcopy with 6 mW beam focusing on it. The times of resolution was adjusted in accordance with the intensity of the Raman scattering.

## 2.3.4. Temperature-programmed reduction

Temperature-programmed reduction (TPR) analysis of samples was investigated by 2910 Automatic chemical adsorption instrument (Micromeritics, United States). Before test, about 100 mg sample was pretreated by argon at 200 °C for 40 min to remove traces of water and cooled down to 60 °C, then heated to 1000 °C with a temperature ramp of 10 °C/min in 10 mol%  $\rm H_2/Ar$  at a flow rate of 30 mL/min.  $\rm H_2$ -TPR was performed with a TCD detector. A cold trap (liquid nitrogen/isopropyl alcohol bath) was used for removing water produced in reduction process to avoid it reached the TCD detector.

## 2.3.5. X-ray photoelectron spectroscopy

X-ray photoelectron spectroscopy (XPS) experiments were recorded using Perkin Elmer PHI-1600 XPS spectrometer with Mg  $K\alpha$  X-ray radiation. The binding energy (BE) was calibrated of C 1 s at 284.6 eV.

## 2.3.6. Transmission electron microscopy (TEM)

All images of high resolution transmission electron microscopy for 10Mo/CeZr catalysts after sulfidation were collected using a

Table 1. Textual properties of the samples.

Catalysts	$S_{\rm BET}~({\rm m}^2/{\rm g})$		Pore size (nm)		Pore volume (cm³/g)	
	Support	Catalyst	Support	Catalyst	Support	Catalyst
10Mo/CeZr-DP	30	24	9.0	8.3	0.082	0.071
10Mo/CeZr-CA	38	17	4.1	11.2	0.097	0.088
10Mo/CeZr-imp	33	11	7.5	19.2	0.093	0.073

Tecnai G2F20 (200 kV) high- resolution transmission electron microscope (TEM) (FEI, Holland). The instrument can reach a maximum resolution of 0.15 nm/200 kV. The powder samples were grounded softly in an agate mortar and dispersed in ethanol by using ultrasonic. A few drops were then deposited on 200 mesh copper grid, being dried overnight for TEM test.

## 2.3.7. Evaluation of catalytic performance

The catalytic activity for sulfur-resistant methanation was performed using a continuous-flow, fixed-bed reactor with stainless steel reactor, inner diameter: 12 mm, length: 700 mm (Terch). The detailed experimental instruments have been introduced in our previous research [13]. Before each catalytic activity test was performed, 3 mL catalyst with particle diameter of 0.43-0.85 mm was sandwiched in the middle of the reactor and the catalyst were subsequently sulfided at 300 °C for 4 h using a 3 vol% H<sub>2</sub>S/H<sub>2</sub> gas mixture (Air Liquide (China) Holding CO, Ltd.) at a flow rate of 100 mL/min. The sulfur-resistant methanation conditions were as follows: syngas ( $H_2/CO = 1.0$ ) composed by 0.3 vol%  $H_2S$ , a gas hourly space velocity of 5000  $h^{-1}$ , 400 °C, and 3 MPa. The outlet gases were quantitatively analyzed by an online gas chromatograph (Agilent 7890A), equipped with six columns (three Porapak-Q (Restek, America)), and one capillary column (Agilent technologies Inc., America), two Carboxen (Restek, America) and three detectors (two TCD and one FID), using N2 or H2 as the carrier gas. And the composition of the outlet mixture was determined by the external standard method. The CO conversion and the distribution for hydrocarbon were calculated using the following equations:

$$\begin{split} X_{\text{CO}} &= \frac{n(\text{CO}_{\text{in}}) - n(\text{CO}_{\text{out}})}{n(\text{CO}_{\text{in}})} \times 100 \% \\ S_{\text{CH}_4} &= \frac{n(\text{CH}_{4_{\text{out}}})}{n(\text{CH}_{4_{\text{out}}}) + n(\text{C}_2 \text{H}_{6_{\text{out}}}) + n(\text{C}_3 \text{H}_{8_{\text{out}}})} \times 100 \% \\ S_{\text{C}_2 \text{H}_6} &= \frac{n(\text{C}_2 \text{H}_{6_{\text{out}}})}{n(\text{CH}_{4_{\text{out}}}) + n(\text{C}_2 \text{H}_{6_{\text{out}}}) + n(\text{C}_3 \text{H}_{8_{\text{out}}})} \times 100 \% \\ S_{\text{C}_3 \text{H}_8} &= \frac{n(\text{C}_3 \text{H}_{8_{\text{out}}})}{n(\text{CH}_{4_{\text{out}}}) + n(\text{C}_2 \text{H}_{6_{\text{out}}}) + n(\text{C}_3 \text{H}_{8_{\text{out}}})} \times 100 \% \end{split}$$

where,  $X_{CO}$ ,  $S_{CH_4}$ ,  $S_{C_2H_6}$ ,  $S_{C_3H_8}$  refer to CO conversion, CH<sub>4</sub>,  $C_2H_6$ , and  $C_3H_8$  selectivity, respectively, n refers to the amount of substance in a gas (CO, CH<sub>4</sub>,  $C_2H_6$  or  $C_3H_8$ ).

## 3. Results and discussion

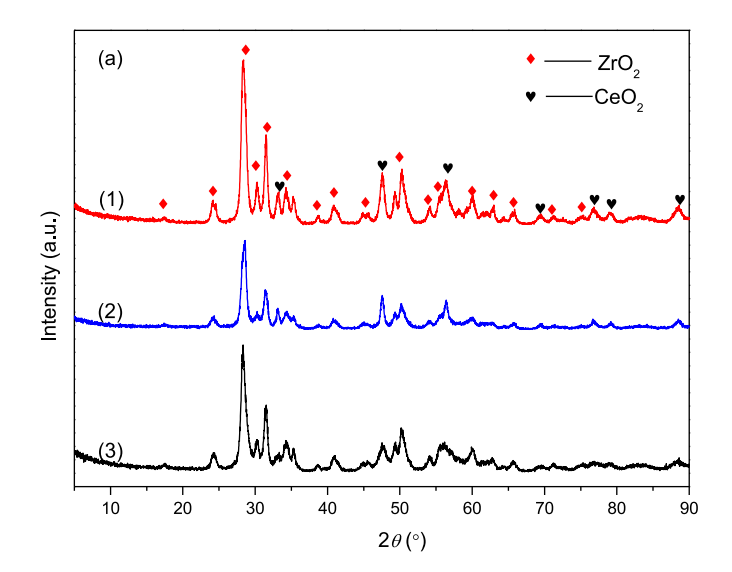
#### 3.1. $N_2$ -physisorption

Table 1 summarizes the structure characteristics of the asprepared catalysts. Generally, the BET surface areas and the pore volume of supported MoO<sub>3</sub> catalysts are lower than those of corresponding supports, which was related to the active component Mo species, blocked the pore of the supports after loading Mo species. Compared to the CeZr-imp, the specific surface area of CeZr-CA support increased that is consisted with Wang et al. [8]. As listed in Table 1, the specific surface areas of CeZr-DP, CeZr-CA and CeZr-imp were 30, 38 and 33 m²/g, respectively. After being loaded 10 wt% MoO<sub>3</sub>, the specific surface areas of the

corresponding catalysts were reduced to 24, 17 and 11 m<sup>2</sup>/g, respectively. It is clear that the specific surface areas of 10Mo/CeZr-DP, 10Mo/CeZr-CA and 10Mo/CeZr-imp catalysts decreased 19.1%, 55.9% and 65.3% compared to their corresponding supports. Both the catalysts of 10Mo/CeZr-DP and 10Mo/CeZr-CA with higher surface area may present higher catalytic activity than the 10Mo/CeZr-imp catalyst.

### 3.2. XRD analysis

The XRD patterns obtained for 10Mo/CeZr samples prepared with different Ce species introduction methods are displayed in Fig. 1(a). For 10Mo/CeZr-DP, the diffraction peaks are ascribed to



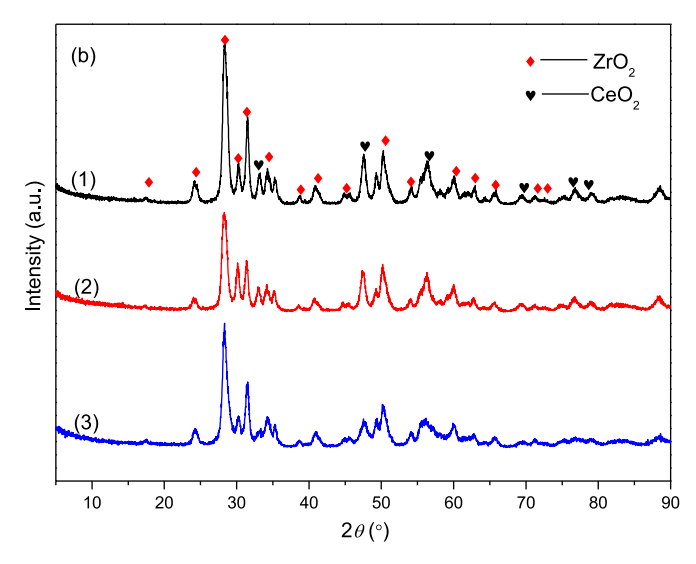


**Fig. 1.** (a) XRD patterns of the 10MoCeZrO<sub>2</sub> catalysts: (1) 10Mo/CeZr-DP, (2) 10Mo/CeZr-CA and (3) 10Mo/CeZr-imp. (b) XRD patterns of the 10Mo/CeZrO<sub>2</sub> catalysts after sulfidation: (1) 10Mo/CeZr-DP, (2) 10Mo/CeZr-CA and (3) 10Mo/CeZr-imp.

Table 2. Characteristics result of catalysts particle size determined by XRD.

Catalysts	Crystallite sizes (nm	)
	ZrO <sub>2</sub> (111)	CeO <sub>2</sub> (200)
10Mo/CeZr-DP	11.7	15.3
10Mo/CeZr-CA	10.8	14.3
10Mo/CeZr-imp	11.7	14.7

 $\rm ZrO_2$  with different crystal phases (PDF: 37-1484, 49-1642) and the cubic fluorite structure of  $\rm CeO_2$  [27] (PDF: 34-0394), respectively. As reported by Sun and Sermon [27], it is evident for a homogeneous distribution of cerium in zirconia. No diffraction peaks corresponding to  $\rm MoO_3$  are detected with the content  $\rm MoO_3$  is 10 wt% indicating that  $\rm MoO_3$  is highly dispersed on the  $\rm CeO_2$ - $\rm ZrO_2$  support or as an amorphous form.

For the other catalyst, 10Mo/CeZr-imp has the similar diffraction peak profile and peak intensity with that of the 10Mo/CeZr-DP catalyst. While the peak intensity of the 10Mo/CeZr-CA catalyst was slightly weaker than those of the other two. The support crystallite sizes were calculated by FWHM method, which were listed in Table 2. By comparing  $D_{XRD}$  of the  $ZrO_2$  and  $CeO_2$  in the support, we found that there is slightly difference between these samples, which is consistent with the XRD peak profile intensity. Because of small difference of three samples, Ce species with different introducing methods showed not significant impact on the bulk phase structure of supports.

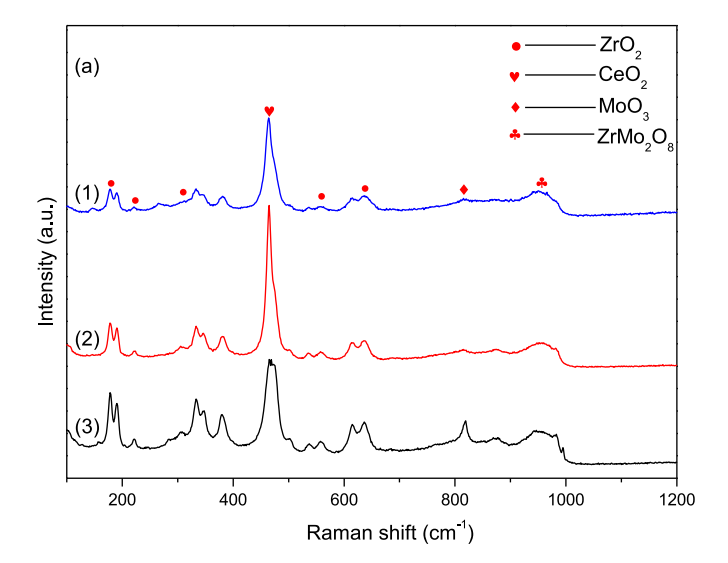
The XRD patterns of the catalysts after sulfidation were also performed and the results were shown in Fig. 1(b). It is clear that the diffraction peaks were similar with the as-prepared 10Mo/CeZr catalysts. Only CeO<sub>2</sub> and ZrO<sub>2</sub> crystal phase were found without obvious diffraction peaks attributed to MoS<sub>2</sub>. This indicated that MoS<sub>2</sub> is highly dispersed on the 10Mo/CeZr catalyst surface after sulfidation.

#### 3.3. Raman analysis

Raman analysis is an effective method to analyze the  $CeO_2$ – $ZrO_2$ materials. Furthermore, it is a powerful technique to determine states of  $MoO_3$  of the catalyst (small crystalline or amorphous). To understand the state of different catalysts, the Raman spectra of various samples prepared in this study have been investigated and the characterization results of all the catalysts samples are presented in Fig. 2(a).

According to the Fig. 2(a), the detection of range of Raman band for all of samples is from 100 cm<sup>-1</sup> to 1200 cm<sup>-1</sup>. The Raman spectrum gives major bands at 270, 315, 472 and 631 cm<sup>-1</sup>, which are assigned to the characteristic bands of *t*-ZrO<sub>2</sub> and Raman bands at 181, 222, 307, 337, 379 and 556 cm<sup>-1</sup> belong to *m*-ZrO<sub>2</sub> [28] indicating that coexistence of different ZrO<sub>2</sub> crystallines. In addition the band at 461 cm<sup>-1</sup> that corresponds to triply degenerate *F*2g mode is viewed as a symmetric breathing mode of oxygen atoms around cerium ions [29,30], and the weak band observed at 600 cm<sup>-1</sup> corresponds to a doubly degenerate longitudinal optical mode of CeO<sub>2</sub> [31,32], this band frequently has been linked to oxygen vacancies in the CeO<sub>2</sub> lattice [29,30]. The Raman results further corroborate with the observations made from XRD measurements.

According to the literature [32], the Raman spectrum of the  $700-1200 \text{ cm}^{-1}$  are corresponding the species associated with compound Mo(VI). In this Raman range there were 748,  $945 \text{ cm}^{-1}$  and  $1000 \text{ cm}^{-1}$  attributed to  $2\text{rMo}_2\text{O}_8$  solid solution. While the bands at 875, 981 and  $818 \text{ cm}^{-1}$  were assigned to amorphous  $\text{MoO}_x$  species and crystalline  $\text{MoO}_3$ , respectively. For Fig. 2(a), in the zone of  $700-1200 \text{ cm}^{-1}$  the Raman spectra clearly showed some differences in the peak intensities of Raman in the three



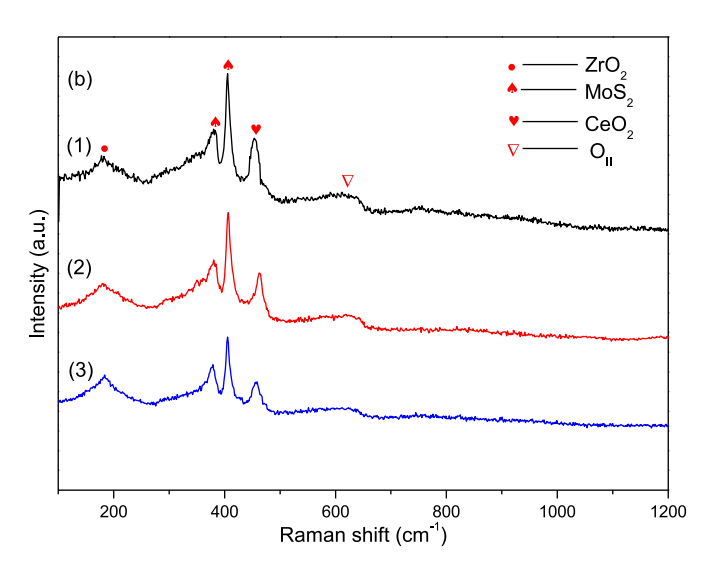


**Fig. 2.** (a) Raman patterns of the 10Mo/CeZr catalysts: (1) 10Mo/CeZr-DP, (2) 10Mo/CeZr-CA and (3) 10Mo/CeZr-imp. (b) Raman patterns of the 10Mo/CeZr catalysts after sulfidation: (1) 10Mo/CeZr-DP, (2) 10Mo/CeZr-CA and (3) 10Mo/CeZr-imp.

samples. The peaks intensity of the 10Mo/CeZr-imp is stronger than that of 10Mo/CeZr-DP. There was a special Raman band at 945 cm<sup>-1</sup> detected for the three different samples and a sharp peak at the band of 818 cm<sup>-1</sup> attributed to crystalline  $\text{MoO}_3$  for the catalyst of 10MoCeZr-imp, and weak Raman peaks at 818 cm<sup>-1</sup> attributed to crystalline  $\text{MoO}_3$  were detected for the catalysts 10Mo/CeZr-CA and 10Mo/CeZr-DP. Combining with XRD analysis (no Mo species diffraction), the supports Mo species is highly dispersed which were not enough to be detected in XRD spectra.

Fig. 2(b) shows the Raman spectra of the catalysts after sulfidation. The bands at 181 cm $^{-1}$  and 460 cm $^{-1}$  were attributed to ZrO $_2$  and CeO $_2$ , respectively. In addition, the bands appearing at 381 and 405 cm $^{-1}$  are ascribed to MoS $_2$  [33,34], while a weak band attributed to defect oxygen (600 cm $^{-1}$ ) was found. The concentration of MoS $_2$  and defect oxygen were reflected by  $(I_2 + I_3)/I_1$ ,  $I_5/I_1$  ( $I_1$ ,  $I_2$ ,  $I_3$  and  $I_5$  is the peak intensity of the bands at 181 cm $^{-1}$ , 381 cm $^{-1}$ , 405 cm $^{-1}$  and 600 cm $^{-1}$ ), which is shown in Table 3. The highest values of  $(I_2 + I_3)/I_1$  and  $I_5/I_1$  were obtained for 10Mo/CeZr-DP catalyst after sulfidation, which presented the optimum sulfur-

**Table 3.** Concentration of  $MoS_2$  and defect oxygen calculated from Raman spectra.

Catalysts	$MoS_2$ concentration $(I_2 + I_3)/I_1$	Defect oxygen concentration $I_5/I_1$
10MoS <sub>2</sub> /CeZr-DP	1.75	0.65
10MoS2/CeZr-CA	1.43	0.61
10MoS <sub>2</sub> /CeZr-imp	0.79	0.54

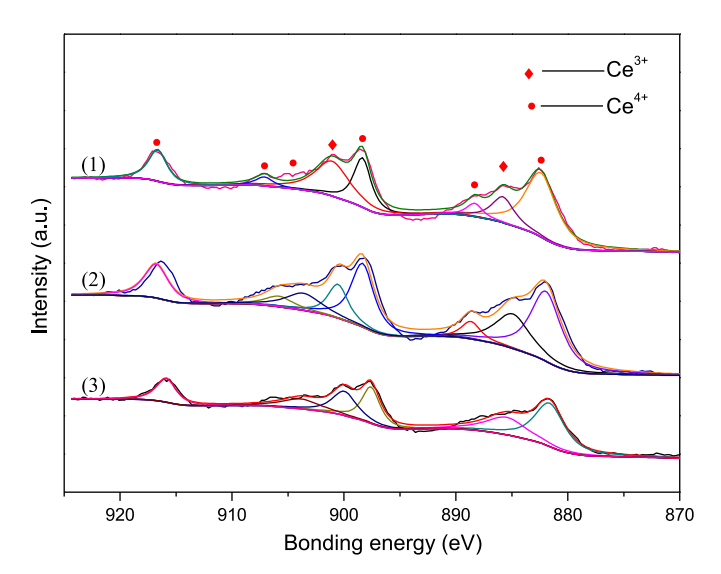


Fig. 3. XPS patterns of the 10Mo/CeZr catalysts: (1) 10Mo/CeZr-DP, (2) 10Mo/CeZr-CA and (3) 10Mo/CeZr-imp.

**Table 4.** Surface elemental composition of Ce and Zr in different catalysts determined by XPS.

Samples	Atomic ratio (Ce/Zr)		$Ce^{3+}/(Ce^{3+}+Ce^{4+})$ (%)
	Bulk	Surface	
10Mo/CeZr-imp	0.018	3.00	13.6
10Mo/CeZr-CA	0.018	3.50	21.3
10Mo/CeZr-DP	0.018	5.09	27.1

resistant methanation activity. So the amounts of  $MoS_2$  and defect oxygen are considered main factors affecting on the methanation activity.

### 3.4. XPS analysis

XPS analysis can verify surface composition and elementary valence states. The complex spectrum of Ce 3d was decomposed into eight peaks according to the previous reports [24,35]. XPS peaks denoted as v(882.3 eV), v'(884.8 eV), v''(888.5) and v'''(898.1 eV) were correspond to Ce  $3d^{3/2}$ , while u(900.6 eV), u'(902.7 eV), u''(907.4 eV) and u'''(916.6 eV) were correspond to Ce  $3d^{5/2}$ . The main peaks marked by v, v'', v''', u, u'', u''' are attributed to the state of Ce<sup>4+</sup> ions, whereas those marked by v' and u' are assigned to the state of Ce<sup>3+</sup> ions [25,35–37]. In other words, the chemical valence of cerium on the surface of 10Mo/CeZr catalysts was mainly in Ce<sup>4+</sup> oxidation state and a small quantity of Ce<sup>3+</sup> co-existed.

The corresponding surface content of 10Mo/CeZr catalysts measured by XPS is listed in Fig. 3 and Table 4. In all the samples, the ratio of cerium to zirconia atomic were lower than that calculated by bulk composition, as indicated by valves in Table 4, which further strengthens the evidence that cerium was enriched on the surface of catalysts. Moreover the surface concentration of  $Ce^{3+}$  could be determined by  $Ce^{3+}$  (%) = (v' + u') /(v + v'' + v''' + u + u'' + u''') [25,36]. The catalyst surface of 10Mo/CeZr-CA possesses larger  $Ce^{3+}$  concentration compared with

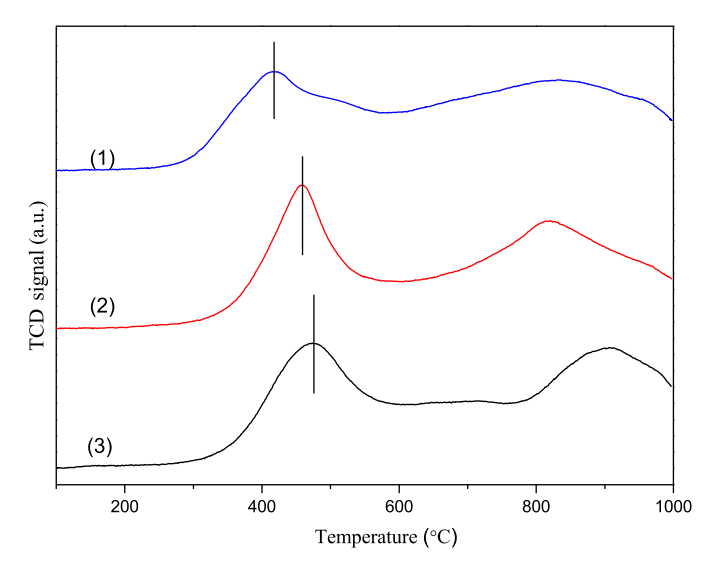


**Fig. 4.** H<sub>2</sub>-TPR patterns of the 10Mo/CeZr catalysts: (1) 10Mo/CeZr-DP, (2) 10Mo/CeZr-CA and (3) 10Mo/CeZr-imp.

 $CeO_2$ – $ZrO_2$ -imp. The adding of citric acid was help to immigrate Ce species from inside to the surface [8], the content of  $Ce^{3+}$  in 10Mo/CeZr-DP was larger than that of the others. The relative intensity of v' and u' to other bands increased from 13.6% to 21.3% and 27.1% with the ratio of Ce/Zr ascending in the surface of 10Mo/CeZr catalysts with three different method. In addition as reported by Paier et al. [38], the exit of  $Ce^{3+}$  can facilitate redox shift  $Ce^{4+}$  into  $Ce^{3+}$  recycles, which is beneficial to the redox reactions. Therefore, it is expected that 10Mo/CeZr-CA and 10Mo/CeZr-DP catalysts should present excellent catalytic performance. The catalyst of 10Mo/CeZr-DP is in promising methanation activity.

## 3.5. H<sub>2</sub>-TPR analysis

The reduction behavior of three kinds of 10Mo/CeZr catalysts was investigated by means of the TPR technique to study the effect of different way of introducing Ce on the reducibility of catalysts. As showed in Fig. 4, there are two broad reduction peaks over temperature range of 300–580 °C and 800–900 °C for the three 10Mo/CeZr catalysts. The lower reduction peak at 300–580 °C is attributed to the reduction of surface CeO<sub>2</sub> crystallites and part of octahedral coordinated Mo<sup>6+</sup> to Mo<sup>4+</sup>, while the higher reduction peak at 800–900 °C is ascribed to the reduction of bulk CeO<sub>2</sub> [39].

Some changes of reduction patterns are observed in different samples. For the 10Mo/CeZr-CA, the lower reduction peak shifts to lower temperature from 476 °C to 455 °C compared to the catalyst of 10Mo/CeZr-imp. While for the 10Mo/CeZr-DP catalyst, the lower reduction peaks moves to lower temperature than the 10Mo/CeZr-CA catalyst. All these observations in TPR profiles demonstrate that the catalysts of 10Mo/CeZr-CA and 10Mo/CeZr-DP appear excellent reducibility compared with 10Mo/CeZr-imp. These also confirmed that 10Mo/CeZr-DP, 10Mo/CeZr-CA catalysts possessed the excellent reducibility, allowing an effective redox cycle during oxidation reactions via Ce<sup>4+</sup>/Ce<sup>3+</sup> redox couple [22,40]. This could improve the reducibility of catalysts [35], which is contributed to higher sulfur-resistant methanation than that of 10Mo/CeZr-imp.

## 3.6. TEM analysis

High resolution transmission electronic microscopy was employed to investigate the morphology and stacking layers of 10Mo/CeZr catalysts after sulfidation, and the results were shown

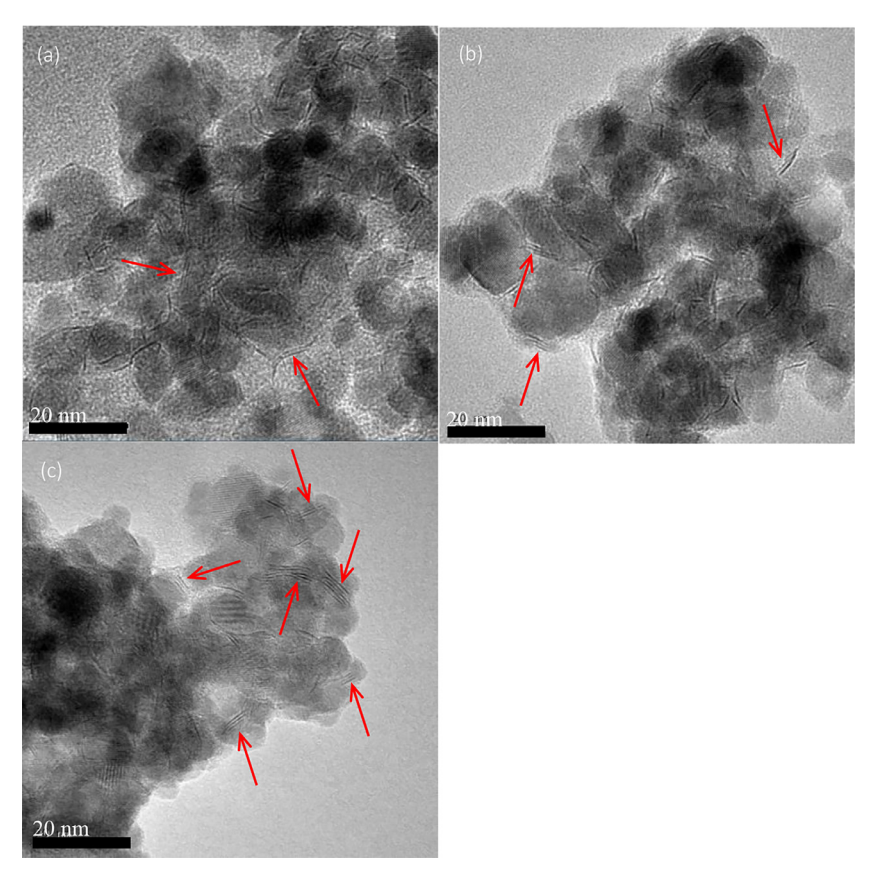


Fig. 5. TEM images of the 10Mo/CeZr catalysts after sulfidation. (a) 10Mo/CeZr-DP, (b) 10Mo/CeZr-CA, (c) 10Mo/CeZr-imp.

in Fig. 5. It is clear that no stacked MoS<sub>2</sub> crystals were found and MoS<sub>2</sub> slabs are straight and short for the 10Mo/CeZr-DP in Fig. 5(a), indicating that the active MoS<sub>2</sub> was highly dispersed on the support. For the 10Mo/CeZr-CA shown in Fig. 5(b), stacked MoS<sub>2</sub> layers were noticed, indicating MoS<sub>2</sub> with multi-layered structure. For the 10Mo/CeZr-imp shown in Fig. 5(c), stacked MoS<sub>2</sub> layers increased further. The previous Raman spectra showed that 10MoS<sub>2</sub>/CeZr-DP exhibited high concentration defective oxygen and MoS<sub>2</sub> site. It was deduced that the defective oxygen is favorable for better dispersion of MoS<sub>2</sub>. As reported [41,42], MoS<sub>2</sub> was the active component of sulfur-resistant methanation and the active site was located at the edge of MoS<sub>2</sub>. Therefore, the well dispersed and monolayered MoS<sub>2</sub> could be favorable for CO conversion.

## 3.7. Evaluation of catalytic performance

Table 5 and Fig. 6 illustrates catalytic performance of 10 wt% Mo/CeZr catalyst prepared by three different methods. Compared to 10Mo/CeZr-imp, the CO conversion of 10Mo/CeZr-CA

Table 5. Catalytic performance of three catalysts.

Samples	CO conversion (%)	Distribution of hydrocarbons (%)		
		CH <sub>4</sub>	C <sub>2</sub> H <sub>6</sub>	C <sub>3</sub> H <sub>8</sub>
10Mo/CeZr-DP	45.3	80.1	18.2	1.7
10Mo/CeZr-CA	40.4	79.3	19.1	1.6
10Mo/CeZr-imp	31.7	79.8	18.5	1.7

and 10Mo/CeZr-DP was 5% and 9%, respectively. And the catalysts 10Mo/CeZr-DP exhibited the excellent catalytic activity for the methanation, which is mainly ascribed to following description: First, the significant factor was the surface concentration of Ce<sup>3+</sup>, which is approximate linear relationship with catalytic activity as shown in Fig. 6. In the previous literature [24], the reducible Ce<sup>3+</sup> helps to the formation of the defect oxygen that could facilitate oxygen mobility, which could promote the dispersion of active components proved by TEM images in Fig. 5. In water-gas shift reaction, reducible Ce<sup>3+</sup> can supply active oxygen species to oxidize CO into CO<sub>2</sub> by temporarily reducing Ce<sup>4+</sup> to Ce<sup>3+</sup> and simultaneously is oxidized again by oxygen from H<sub>2</sub>O [22,40]. As reported by Happel et al. [11], the sulfur-resistant methanation was coupled with hydrogenation of carbon monoxide and carbon monoxide water-gas shift reaction, where hydrogenation of carbon monoxide was viewed as an irreversible reaction while carbon monoxide water-gas shift reaction was a reversible reaction. These two reactions act synergistically; hence we can improve the methanation activity through increased WGS reaction. Above all three catalysts the amount of the Ce3+/Ce4+ concentration at the interface: 10Mo/CeZr-DP > 10Mo/CeZr-CA > 10Mo/CeZr-imp. Second, it is well known that the reducibility has beneficial in redox reactions [38]. The reducibility for this research 10Mo/CeZr-DP > 10Mo/CeZr-CA > 10Mo/CeZr-imp was confirmed from H<sub>2</sub>-TPR. In addition, for the 10Mo/CeZr catalysts after sulfidation, 10Mo/CeZr-DP provided higher surface MoS<sub>2</sub> concentration and well dispersed MoS<sub>2</sub>, which were responsible for higher activity of 10Mo/CeZr-DP catalyst than the other two catalysts.

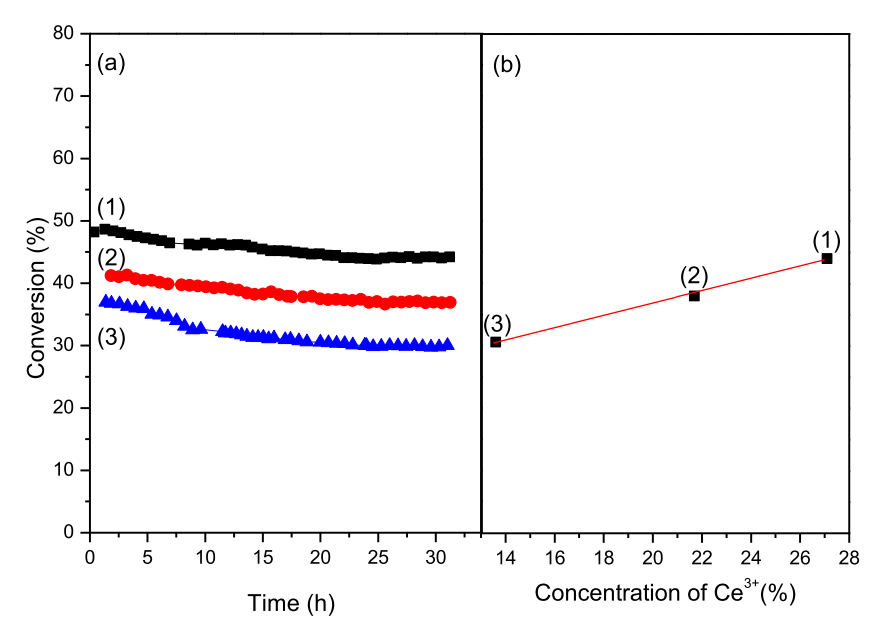


Fig. 6. (a) Catalytic performance of the 10Mo/CeZr catalysts: (1) 10Mo/CeZr-DP, (2) 10Mo/CeZr-CA and (3) 10Mo/CeZr-imp; (b) the surface concentration of Ce<sup>3+</sup>: (1) 10Mo/CeZr-DP, (2) 10Mo/CeZr-CA and (3) 10Mo/CeZr-imp.

## 4. Conclusions

The different introduction of Ce species in  $CeO_2$ – $ZrO_2$  supports for supported Mo/CeZr catalysts and their methanation performances were reported. The syngas methanation activity for 10Mo/CeZr-CA, 10Mo/CeZr-DP reaches up 40.4% and 45.3%, respectively. These are higher than that of 10Mo/CeZr-imp. And 10Mo/CeZr-DP exhibited the excellent catalytic performance for sulfur-resistant methanation.

The characterized results indicated that active component Mo species have a good dispersion on  $CeO_2$ – $ZrO_2$  supports with different Ce adding method. However, these catalysts exhibit different properties in terms of surface area, Ce/Zr ratio, amounts of reducible  $Ce^{3+}$  and active component  $MoS_2$  on the catalyst surface and the reducibility, which could have important effect on methanation activity. The catalytic performance showed good correlation with  $Ce^{3+}$  and  $MoS_2$  concentration of catalysts. The catalysts with higher concentration of reducible  $Ce^{3+}$  and higher  $MoS_2$  content are responsible for excellent sulfur-resistant activity. In addition, the excellent reducibility of ceria via the redox shifts between  $Ce^{4+}/Ce^{3+}$  also leads to an improvement in sulfur-resistant methanation activity.

## Acknowledgments

Financial supports from the National High Technology Research and Development Program of China (863 Project) (2015AA050504) and the National Natural Science Foundation of China (21576203) are gratefully acknowledged.

## References

- [1] J.J. Gao, C.M. Jia, J. Li, M.J. Zhang, F.N. Gu, G.W. Xu, Z.Y. Zhong, F.B. Su, J. Energy Chem. 22 (6) (2013) 919–927.
- [2] H.Y. Wang, Z.H. Li, E.D. Wang, C. Lin, Y.G. Shang, G.Z. Ding, X.B. Ma, S.D. Qin, Q. Sun, J. Nat. Gas Chem. 21 (6) (2012) 767–773.
- [3] Z.H. Li, Y. Tian, B.W. Wang, X.B. Ma, J. Energy Chem. 23 (5) (2014) 625-632.
- [4] J. Kopyscinski, T.J. Schildhauer, S.M.A. Biollaz, Fuel 89 (8) (2010) 1763–1783.
- [5] Y.Z. Wang, R.F. Wu, Y.X. Zhao, Catal. Today 158 (3) (2010) 470-474.
- [6] R.W. Fowler Jr., C.H. Bartholomew, Ind. Eng. Chem. Prod. Res. Dev. 18 (4) (1979) 339–347.
- [7] A.W.A.B. Wan, M.Y. Othman, R. Ali, C.K. Yong, Catal. Lett. 128 (1) (2009) 127–136

- [8] B.W. Wang, D.J. Meng, W.H. Wang, Z.H. Li, X.B. Ma, J. Fuel Chem. Technol. 4 (12) (2016) 1479–1484.
- [9] B.W. Wang, Y.Q. Yao, S.H. Liu, Z.Y. Hu, Z.H. Li, X.B. Ma, Fuel Process. Technol. 138 (2015) 263–270.
- [10] P.Y. Hou, H. Wise, J. Catal. 93 (2) (1985) 409-416.
- [11] J. Happel, M.A. Hnatow, L. Bajars, Gas research Institute, Chicago, III.US4491639. 1985.
- [12] B.W. Wang, Y.Q. Yao, M.H. Jiang, Z.H. Li, X.B. Ma, S.D. Qin, Q. Sun, J. Energy Chem. 23 (1) (2014) 35–42.
- [13] B.W. Wang, G.Z. Ding, Y.G. Shang, J. Lv, H.Y. Wang, E.D. Wang, Z.H. Li, X.B. Ma, S.D. Qin, Q. Sun, Appl. Catal. A: Gen. 431-432 (2012) 144-150.
- [14] D.J. Meng, B.W. Wang, Z. Liu, W.H. Wang, Z.H. Li, X.B. Ma, J. Energy Chem. 26 (2017) 368–372.
- [15] M.H. Jiang, B.W. Wang, J. Lv, H.Y. Wang, Z.H. Li, X.B. Ma, S.D. Qin, Q. Sun, Appl. Catal. A: Gen. 466 (10) (2013) 224–232.
- [16] M.H. Jiang, B.W. Wang, Y.Q. Yao, Z.H. Li, X.B. Ma, S.D. Qin, Q. Sun, Appl. Surf. Sci. 285 (1) (2013) 267–277.
- [17] M.H. Jiang, B.W. Wang, Y.Q. Yao, H.Y. Wang, Z.H. Li, X.B. Ma, S.D. Qin, Q. Sun, Catal. Commun. 35 (35) (2013) 32–35.
- [18] B.W. Wang, G.Z. Ding, J. Lv, H.Y. Wang, E.D. Wang, Z.H. Li, X.B. Ma, S.D. Qin, Q. Sun, React. Kinet. Mech. Catal. 106 (2) (2012) 495–506.
- [19] S. Damyanova, M.A. Centeno, L. Petrov, P. Grange, Spectrochim. Acta A 57 (12) (2001) 2495–2501.
- [20] N. Laosiripojana, S. Assabumrungrat, Appl. Catal. B: Environ. 60 (1–2) (2005) 107–116.
- [21] D.W. Jeong, H.S. Potdar, H.S. Roh, Catal. Lett. 142 (4) (2012) 439–444.
- [22] D.W. Jeong, H.S. Potdar, J.O. Shim, W.J. Jang, H.S. Roh, Int. J. Hydrogen Energy 38 (11) (2013) 4502–4507.
- [23] D.W. Jeong, W.J. Jang, J.O. Shim, W.B. Han, H.S. Roh, U.H. Jung, L.Y.N Wang, Renew. Energy 65 (2014) 102–107.
- [24] D.W. Jeong, W.J. Jang, H.S. Na, J.O. Shim, A. Jha, H.S. Roh, J. Ind. Eng. Chem. 27 (2015) 35–39.
- [25] D.W. Jeong, H.S. Na, J.O. Shim, W.J. Jang, H.S. Roh, Catal. Sci. Technol. 5 (7) (2015) 3706–3713.
- [26] P. Fornasiero, G. Balducci, R.D. Monte, J. Kašpar, V. Sergo, G. Gubitosa, A. Ferrero, M. Graziani, J. Catal. 164 (1) (1996) 173–183.
- [27] Y.H. Sun, P.A. Sermon, J. Mater. Chem. 6 (6) (1996) 1025–1029.
- [28] C. Li, M.J. Li, J. Raman Spectrosc. 33 (5) (2002) 301–308.
- [29] X.M. Lin, L.P. Li, G.S. Li, W.H. Su, Mater. Chem. Phys. 69 (1) (2001) 236– 240.
- [30] B.M. Reddy, K.N. Rao, G.K. Reddy, A. Khan, S. Park, J. Phys. Chem. C 111 (51) (2007) 18751–18758.
- [31] J.R. Mcbride, K.C. Hass, B.D. Poindexter, W.H. Weber, J. Appl. Phys. 76 (4) (1994) 2435–2441.
- [32] B. Samaranch, G. Clet, M. Houalla, N. Homs, Chem. Mater. 18 (2006) 1581–1586.
- [33] É. Blanco, P. Afanasiev, G. Berhault, D. Uzio, S. Loridant, C. R. Chim. 19 (10) (2016) 1310–1314
- [34] M.T. Claure, S.H. Chai, S. Dai, K.A. Unocic, F.M. Alamgir, P.K. Agrawal, C.W. Jones, J. Catal. 324(2015)88–97.
- [35] S.M. Li, Q.L. Hao, R.Z. Zhao, D.L. Liu, H.Z. Duan, B.J. Dou, Chem. Eng. J. 285 (2016) 536–543.

- [36] A.E. Nelson, K.H. Schulz, Appl. Surf. Sci. 2103 (3–4) (2003) 206–221.[37] B.W. Wang, C.M. Chi, M. Xu, C. Wang, D.J. Meng, Chem. Eng. J. 322 (2017) 679–692.
- [38] J. Paier, C. Penschke, J. Sauer, Chem. Rev. 113 (6) (2013) 3949–3985. [39] F. Giordano, A. Trovarelli, C.D. Leitenburg, M. Giona, J. Catal. 193 (2) (2000) 273–282.
- [40] C. He, Y.K. Yu, Y. Lin, N.L. Qiao, J.J. Li, Q. Shen, W.J. Yu, J.S. Chen, Z.P. Hao, Appl. Catal. B: Environ. 147 (147) (2014) 156–166.
  [41] M.H. Jiang, B.W. Wang, Y.Q. Yao, Z.H. Li, X.B. Ma, S.D. Qin, Q. Sun, Catal. Sci. Technol. 3 (10) (2013) 2793–2800.
  [42] Z.H. Li, H.Y. Wang, B.W. Wang, X.B. Ma, Front. Chem. Sci. Eng. 9 (1) (2015) 232.20.
- 33–39.